Open Access Journal
Journal of Power Technologies 93 (4) (2013) 247–256
journal homepage:papers.itc.pw.edu.pl

An Investigation of Oxide Layer Impact on Heat Transfer in a Fuel Element of the MARIA Reactor

Szymon Jerzy Suchcicki[*,a], Nikołaj Uzunow[a], Krzysztof Pytel[b], Władysław Mieleszczenko[b], Alojzy Mołdysz[b]

[a]*Institute of Heat Engineering, Warsaw University of Technology*
Nowowiejska 21/25, 00-665 Warsaw, Poland
[b]*National Centre for Nuclear Research*
A. Sołtana 7, 05-400 Otwock, Poland

Abstract

Within the framework of test fuel examination one of the fuel elements was irradiated to a high level of burnup (c. 60%). Post-irradiation examinations proved that under high burnup local detachment of the oxide layer from the fuel element cladding occurs. Unilateral detachment of the oxide layer, which has strong insulation properties, from the cladding surface may cause disruption to conditions for heat removal from the fuel. This effect was numerically modeled using ANSYS FLUENT code. The numerical results confirmed the existence of heat flux redistribution in the spot where the oxide layer detached. Because the phenomenon of the oxide layer breaking away appears at high fuel burnup, the thermal loads are lower than in most thermally loaded fuel elements so the safety margins for fuel operation are preserved.

Keywords: MARIA reactor, Oxide layer

1. Introduction

During operations of the MARIA reactor a layer of hydrated aluminum oxide is created on the surface of fuel elements' cladding, termed an oxide layer. It is characterized by very low thermal conductivity. Its thickness increases gradually over time and for a certain length of time this layer adheres strictly to the cladding. On achieving the thickness of several tens of μm it breaks away and a creation process starts anew.

[*]Corresponding author
Email addresses: szymon.suchcicki@gmail.com (Szymon Jerzy Suchcicki[*]), uzunow@itc.pw.edu.pl (Nikołaj Uzunow), krzysztof.pytel@ncbj.gov.pl (Krzysztof Pytel), orb1@cyf.gov.pl (Władysław Mieleszczenko), alek.moldysz@cyf.gov.pl (Alojzy Mołdysz)

The rate of oxide layer accretion mainly depends in terms of temperature on the water–oxide boundary and on the pH of the cooling water, whilst it does not depend on pressure and the velocity of water flow. The rate of increase in oxide layer thickness is determined by means of the Arrhenius formula [1]:

$$v_b = v_0 \exp\left(-\frac{E_b}{k_B T}\right) \tag{1}$$

where: v_0—chemical reaction constant, E_b—chemical reaction activation energy, k_B—Boltzmann constant and T—temperature given in K degrees.

This kind of relationship was proven earlier by American experimental examinations within the range of pH= $5 \div 5.5$ and the matching constants are:

$$v_0 = 7.23 \cdot \frac{10^6 \mu m}{d} \tag{2}$$

$$E_b = 0.56\, eV \tag{3}$$

$$E_b/k_B = 6490\, K \tag{4}$$

One of the two MC fuel elements that were tested in the MARIA reactor is presented in this article. This element worked in the reactor from August 11, 2009 to January 21, 2011 and reached 5899 MWh burnup, while the second one worked in the reactor from October 20, 2009 to August 17, 2010 and reached 4025 MWh burnup. Detachment of the oxide layer from the outer surface of fuel element was noticed only in the first element, which reached higher burnup.

Figure 1 shows photographs of the MC fuel element cladding surface in a place where the cladding is totally covered by the oxide layer and in a place of partial separation of this layer.

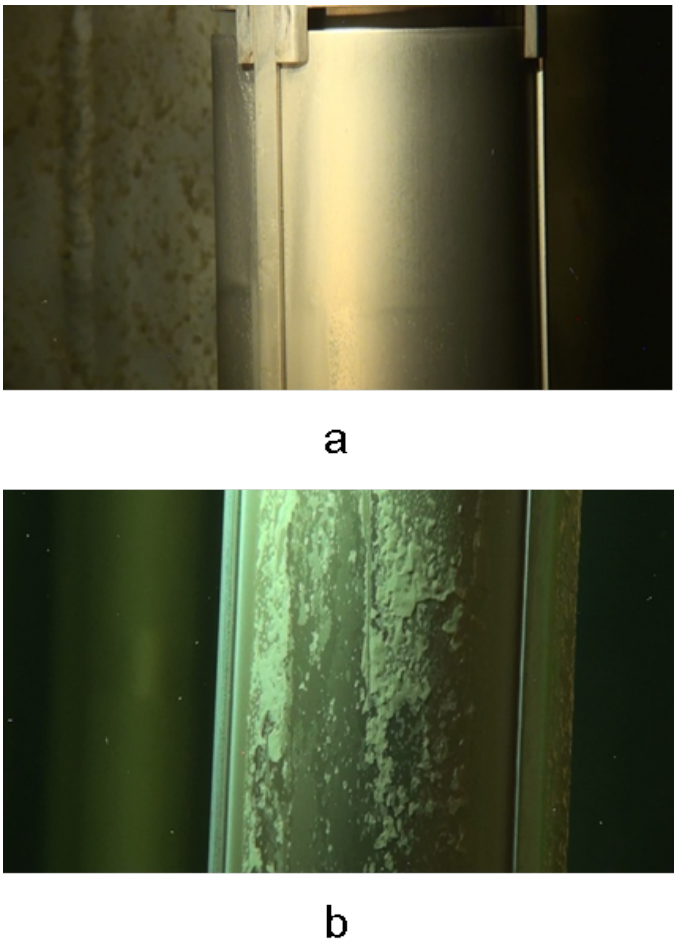

Figure 1: Photographs of the external surface of the MC fuel element's tube No. 6: a—top part of element (cladding totally covered by oxide layer); b—central part of element (cladding with oxide layer partially detached) [1]

2. Description of calculations

A number of computer simulations were performed to determine temperatures and heat flux densities on fuel element cladding. All calculations were made for a selected fragment of the 6th tube for the MC fuel element. This type of fuel element consists of 15 bent fuel plates joined in 5 fuel tubes.

Figure 2 presents the zone, marked by red lines, for which a series of calculations was performed using ANSYS FLUENT 13.0 code. Although one can see only 2 dimensions of the zone in this drawing, it is considered as a volume.

Tube No. 6 was chosen since the highest temperatures are present on its surfaces. Moreover, from that tube a fragment of 10 cm length was chosen (the total length of the fuel contained tube segment is 100 cm) for which the greatest heat generation is recorded, because presumably the oxide layer will break away earliest in this place. The inner surface of the 6th tube is of particular interest, because slightly greater temperatures occur there than on the outer surface. Accordingly, the calculations were made for the events featuring detachment of oxide layer fragments only for the inner side of the 6th tube.

The three-dimensional region consists of fuel tube fragments over the 10 cm length and water layers on both of its sides. Water in both gaps flows downwards. The region encloses half of the thickness of the aluminum connecting the link and half of the width of the fuel plate. From outside this region it is constrained by the inner surface of fuel channel tube and from inside by an arc passing through the center of the water gap between tubes 5 and 6.

As shown in Figure 2, the tube consists of three regions separated from each other by aluminum connectors. Detachment of the oxide layer fragment from the cladding surface in one of these three regions has minimal impact on heat exchange in the other regions. Besides, it was assumed that oxide layer detachment will occur exactly at the halfway

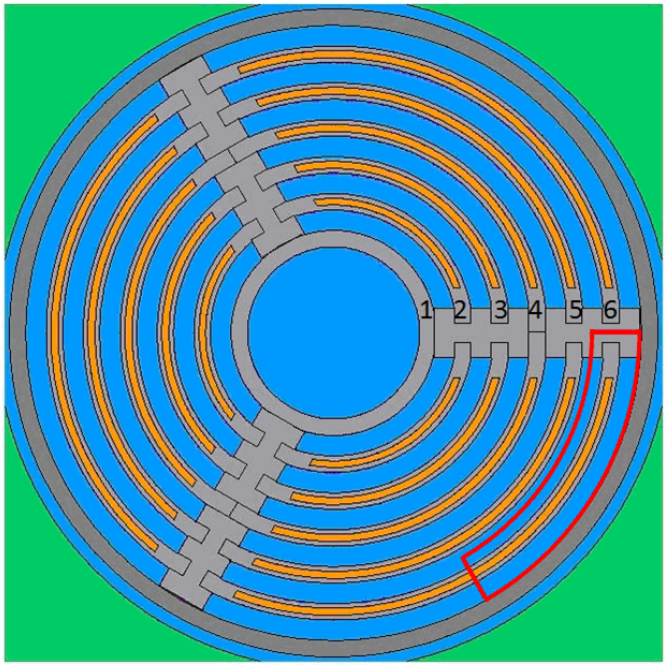

Figure 2: Cross-section for the fuel element with marked region being analyzed [2]

point of the fuel plate width on the inner surface of the 6th tube and at the halfway point along the length of the examined segment, and that it will be circular in shape.

Accordingly, calculations were made only for 1/6 of the circumference of the 6th tube. The plates of symmetry are placed in the center of the aluminum connector and at the halfway point of the fuel plate width. The region analyzed is constrained from the inside by an arc passing through the water gap center, as there was assumed to be no heat exchange between the water on one side of this arc and the water on the other side. This is substantiated by the fact that heat is generated in tubes 5 and 6. Due to this assumption a symmetry condition indicating no heat exchange through this surface was applied on the surface at the halfway point between these two tubes.

The calculations were performed for cases when:

a) Oxide layer is distributed on both sides of the tube (symmetrical layer);

b) Oxide layer appears only on the outer side of the tube (asymmetrical layer with total separation on the inner side);

c) Oxide layer in a circular shape with a diameter of 10 mm was breaking away on the inner side;

d) Oxide layer in a circular shape with a diameter of 5 mm was breaking away on the inner side;

e) Detachment of oxide layer in a circular shape with a diameter of 2 mm occurred on the inner side.

The regions' geometry as well as the three-dimensional discretization lattices for all the above cases were created using GAMBIT code.

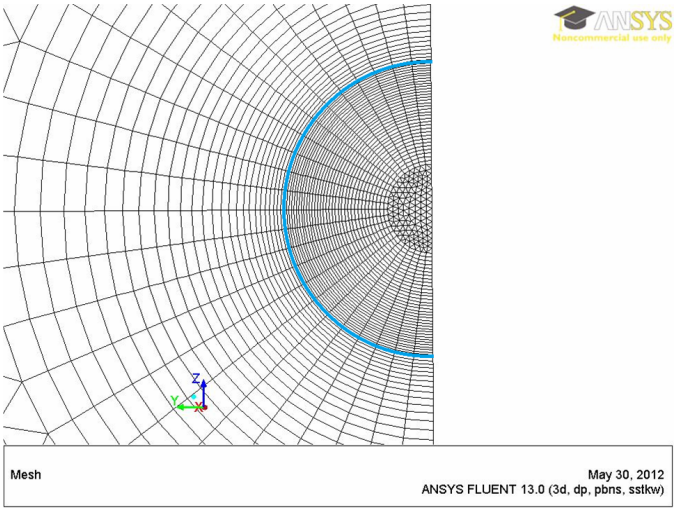

Figure 3: Lateral view of the lattice in the hole and in the near region for the detachment diameter of 2 mm with marked boundary line of oxide layer detachment [2]

The lattices generated for cases a) and b) consist exclusively of hexahedral elements, whereas the lattices for the other cases, because of the geometrical complication, consist of both hexahedral and pentahedral elements (prism with a triangular base). Pentahedral elements were used in the middle of a hole created as an effect of oxide layer detachment, as illustrated in Figure 3, and in an area not adjacent to the hole. Due to the presence of large gradients of sought values near the border of the detachment (blue line in Fig. 3) hexahedral elements were used there. Such elements were also used in the area of the aluminum connector and in the fuel plate near to the connector.

The numbers of cells in discretization lattices for cases a), b), c), d) and e) are: 531300, 506000, 1502032, 1271536 and 1423436.

Calculations were performed for the steady state.

It was assumed that the detachment of the oxide layer does not cause a reduction in the thickness of the aluminum fuel cladding.

Calculations were performed for an oxide layer with a thickness of 50 μm.

It has been taken into consideration that there is no thermal contact resistance between the fuel layer and aluminum cladding as well as between the cladding and oxide layer because these materials fit tightly together.

As the gradient for the linear generation of thermal power in the selected segment of the 6th tube is very small, it was assumed that the linear thermal power generation is a constant value.

Heat exchange does not occur in the spots where there are surfaces of symmetry. Moreover, the lack of heat exchange was assumed through the upper and lower areas of the fuel plate and aluminum connector and through the outer surface of the region.

The following boundary conditions were applied:

- "velocity-inlet" on the inlet surfaces where inlet temperatures and inlet velocity profiles were declared (shown in light blue in the image);
- "pressure-outlet" on the outlet surfaces where the values of static outlet pressure were declared;
- "symmetry" on the inner surface of the region to be investigated as well as on the two side surfaces adjacent to it (shown in yellow in the image);
- "wall" on surfaces of all solid bodies (shown in black) beyond the two side surfaces of the linking connector and the oblong fuel plate for which the symmetry condition was applied.

Figure 4 shows that for the outer surface of the considered region the "wall" condition was applied. This surface represents an inner wall of the fuel channel which was described earlier.

If the "wall" type condition is to be used, a zero value is set for heat flux penetration through the surface for which it has been declared on condition that it is a surface placed on the edge of the region (e.g. outer surface). Otherwise, if the surface is located between two zones the coupled thermal condition is assumed and then heat may be exchanged through the surface between the zones adjacent to it.

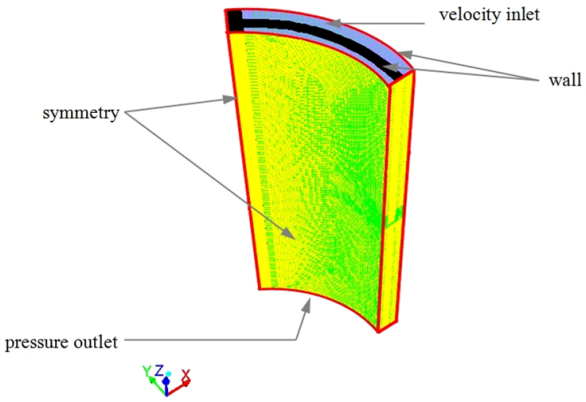

Figure 4: Region to be considered along with boundary conditions marked [2]

For the calculations the following data were used:

- Linear generation of thermal power inside the fuel layer: Q_l = 6.79 kW/cm (for the whole tube circumference);
- Volumetric capacity of the internal heat source in fuel layer: $S_b = Q_l/(6A)$ = 4.5918 GW/m^3 (it was divided by 6 because the calculations refer to 1/6 of tube perimeter), where A is half the surface area of the cross-section for the fuel layer for the 6th plate of the fuel tube;
- On the inner wall side:
  - Inlet temperature: T_{6in} = 64.3°C;
  - Mass flux: m_6 = 631.1 g/(cm^{2}s);
- On the outer wall side:
  - Inlet temperature: T_{7in} = 56.3°C;
  - Mass flux: m_7 = 568.8 g/(cm^{2}s);
- The inlet pressure on both sides is 1.61 MPa;
- Thermal conductivity of the aluminum cladding is: λ_{Al} = 132 W/(mK);
- Thermal conductivity of the fuel layer is: λ_f = 60 W/(mK);

- Thermal conductivity of the oxide layer is: λ_b = 2.25 W/(mK);
- Thermal conductivity, density, specific heat and dynamic viscosity of water were taken from tables [3, 4] and they depend on temperature, their values were defined by linear interpolation.

As the water flow through the region to be analyzed is turbulent, it was necessary to use the Reynold's equations, which were the averaged Navier-Stoke's equations. In this case the ANSYS FLUENT code applies the following conservation equations [5]:

Mass conservation equation (continuity equation):

$$\frac{\partial u_i}{\partial x_i} = 0 \tag{5}$$

Equation for conservation of momentum:

$$\rho \frac{\partial}{\partial x_j}\left(u_i u_j\right) = -\frac{\partial p}{\partial x_i} + \frac{\partial}{\partial x_j}\left[\mu\left(\frac{\partial u_i}{\partial x_j} + \frac{\partial u_j}{\partial x_i} - \frac{2}{3}\delta_{ij}\frac{\partial u_i}{\partial x_i}\right)\right] + \frac{\partial}{\partial x_j}\left(-\rho\overline{u_i' u_j'}\right) \tag{6}$$

were

$$\delta_{ij} = \begin{cases} 1 & i = j \\ 0 & i \neq j \end{cases} \tag{7}$$

Equation for conservation of energy for liquid:

$$\nabla \cdot \left(\vec{v}\left(\rho E + p\right)\right) = \nabla \cdot \left(k_{eff} \nabla T\right) \tag{8}$$

where: k_{eff}—effective thermal conductivity,

$$k_{eff} = k + k_t \tag{9}$$

where k_t is the turbulent thermal conductivity.

For the solids the equation for conservation of energy takes the following form:

$$\nabla \cdot (k \nabla T) + S_h = 0 \tag{10}$$

where S_h is the volumetric capacity for the inner heat source.

In equations Einstein's contracted summation notation was applied in which the indexes to be repeated denote summation in the entire range of their variation.

To close Reynold's equations it is necessary to apply one of the turbulence models. The two equations turbulence model SST-kω (Shear Stress Transport k-ω) was applied, because this model is recommended for cases with boundary layer separation, and in 3 analyzed cases with partial detachment of the oxide layer the phenomenon of hydrodynamic boundary layer separation occurs near the hole's edge. The SST-kω turbulence model is a blend of k-ω and k-ε models. Near the wall it uses the k-ω model whereas in regions further away from the wall it uses the k-ε model, and thereby avoids the common k-ω problem that the model is too sensitive to the inlet free-stream turbulence properties.

3. Computer simulation results

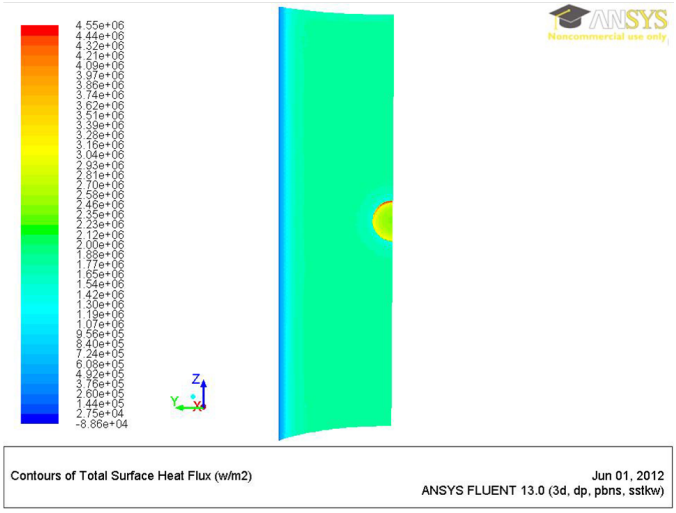

Figure 5: Heat flux density on the inner side of the 6th tube for the detachment diameter of 10 mm [2]

Figures 5–10 present the heat flux densities on the inner side of the 6th tube and in the hole occurring after detachment of the oxide layer for 3 diameters. An increase in heat flux density inside the hole can be observed, whereas in the direct vicinity of detachment a decrease in this quantity can be observed.

Maximum values of heat flux density grow as the hole diameter in the oxide layer decreases.

It is evident that the highest values appear in the upper part of the hole. This is caused by the vortex created in this spot, which is shown in Figures 12–14. These figures show the velocity vectors of water on the inner side of the 6th fuel tube. The vectors are presented in the symmetry plane shown in Figure 11.

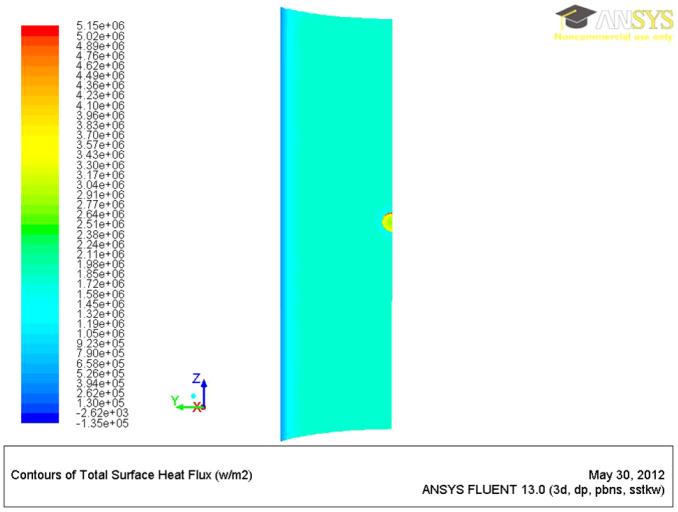

Figure 6: Heat flux density on the inner side of the 6th tube for the detachment diameter of 5 mm [2]

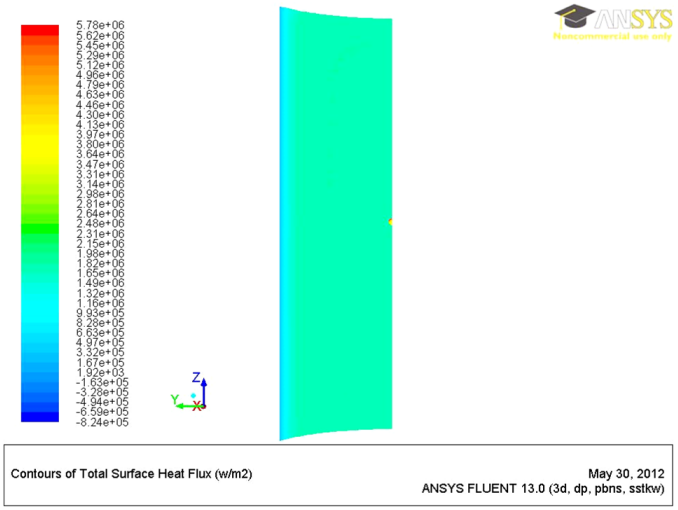

Figure 7: Heat flux density on the inner side of the 6th tube for the detachment diameter of 2 mm [2]

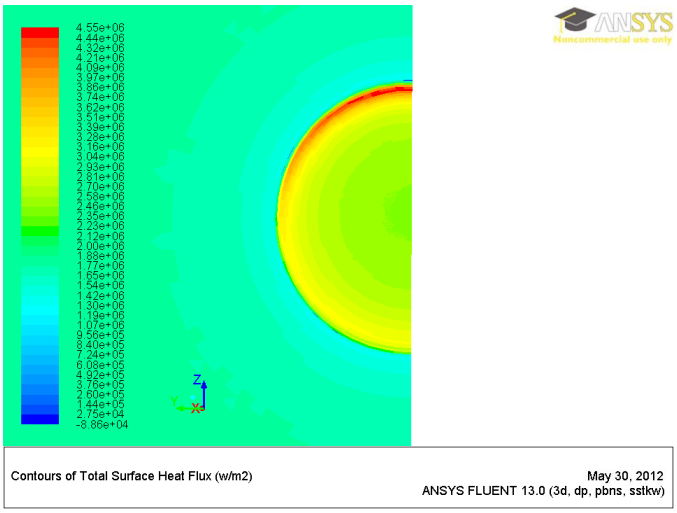

Figure 8: Heat flux density in the hole and in the near region for the detachment diameter of 10 mm [2]

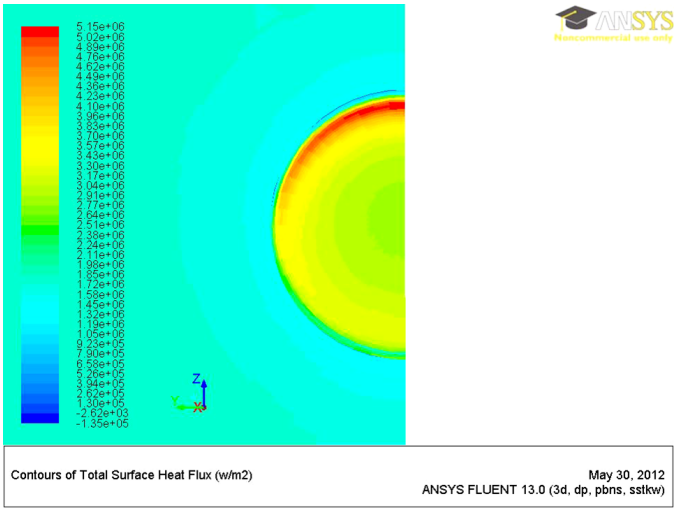

Figure 9: Heat flux density in the hole and in the near region for the detachment diameter of 5 mm [2]

Figures 15–20 present the temperature distributions on the inner side of the 6th tube as well as in the hole created after detachment of the oxide layer for 3 diameters. An increase in temperature inside the hole can be observed, while in the direct vicinity of the detachment a decrease in this quantity can be observed.

Maximum values of temperature grow as the hole diameter in oxide layer decreases.

Figures 21–22 show the relative heat flux densities and the relative temperatures as a ratio of maximum values of heat flux densities and temperatures in investigated cases c), d) and e) to maximum values of these variables in the symmetric layer. The marked points are results of the investigated cases and the line is polynomial regression.

To verify whether boiling of water will not occur in the fuel elements channels, the temperature has to be determined for onset of subcooled bubble boiling T_{ONB} (Onset Nucleate Boiling) as well the ONBR parameter [6] for the line of holes' symmetry:

$$ONBR = \frac{T_{ONB} - T_{in}}{T_{c,max} - T_{in}} \tag{11}$$

where $T_{c,max}$ and T_{in} are the maximum temperature for fuel element cladding and water temperature at the inlet to the fuel channel, respectively.

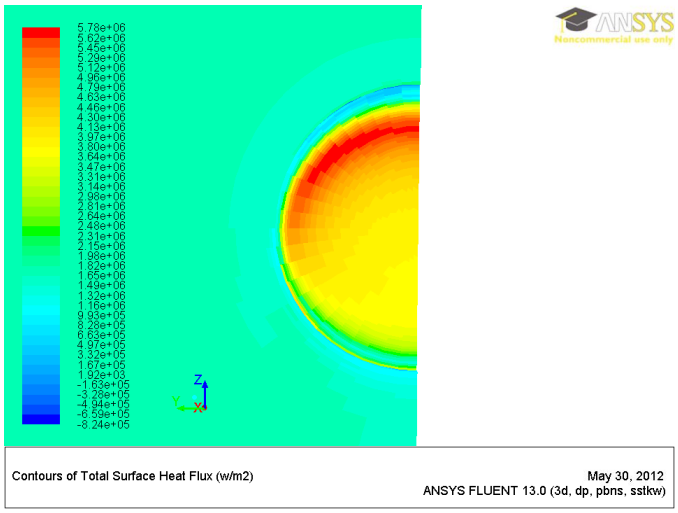

Figure 10: Heat flux density in the hole and in the near region for the detachment diameter of 2 mm [2]

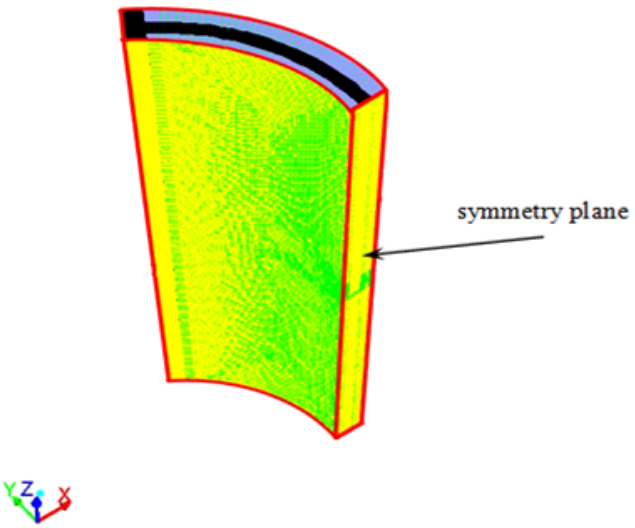

Figure 11: Symmetry plane

In the safety analyses two safety limits are used [1]: exclusion of surface boiling on the fuel element cladding as well as providing the limit $ONBR > 1.2$. The onset temperature for subcooled bubble boiling T_{ONB} is determined by means of the correlation of Forster and Greif [1]:

$$T_{ONB} = T_{SAT} + 0.182 \frac{q^{0.35}}{p^{0.23}} \qquad (12)$$

where: T_{SAT}—saturation temperature, q—heat flux on the wall [W/m^2], p—water pressure [bar].

Figure 23 presents the minimal values of $ONBR$ parameter for 3 cases of oxide layer detachment.

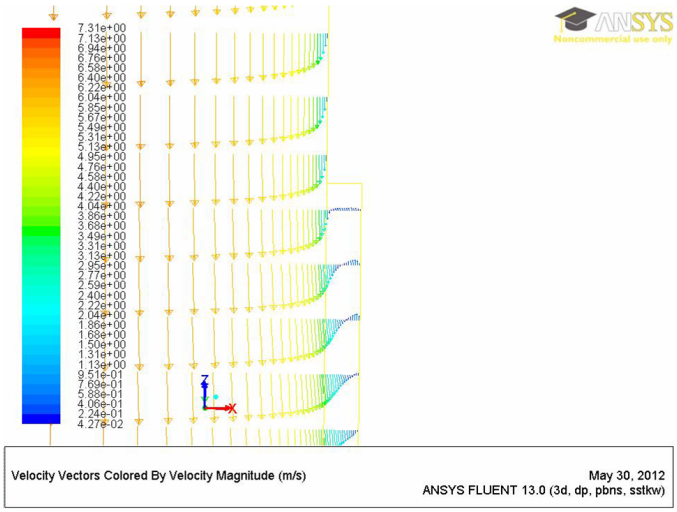

Figure 12: Velocity vectors on the symmetry plane at the top of the hole for the hole diameter of 10 mm [2]

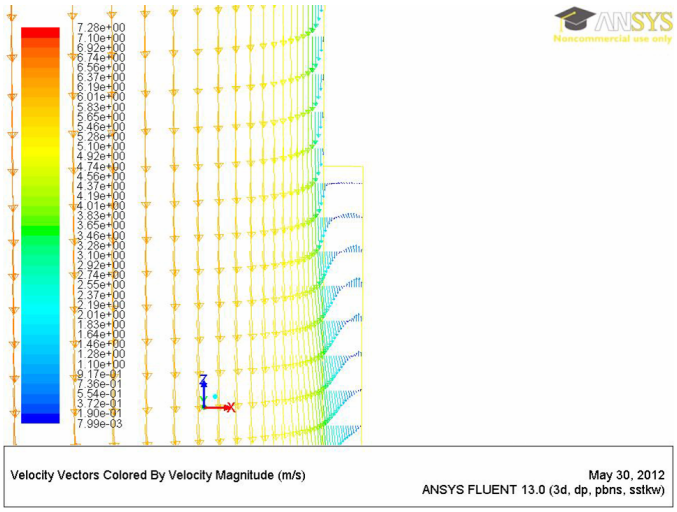

Figure 13: Velocity vectors on the symmetry plane at the top of the hole for the hole diameter of 5 mm [2]

4. Conclusions

An analysis of the computer simulations allow one to formulate the following conclusions:

- Occurrence of oxide layer detachment significantly affects the distribution of heat flux density and temperature on the surface of fuel cladding;
- Values of heat flux density and temperature increase substantially in the separation spots;

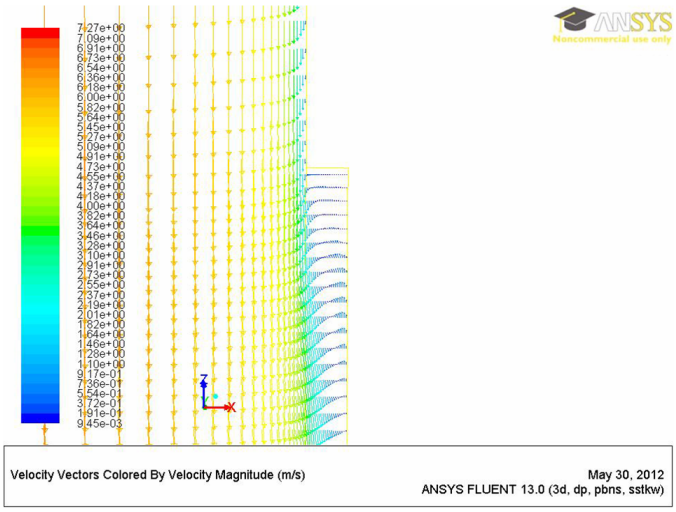

Figure 14: Velocity vectors on the symmetry plane at the top of the hole for the hole diameter of 2 mm [2]

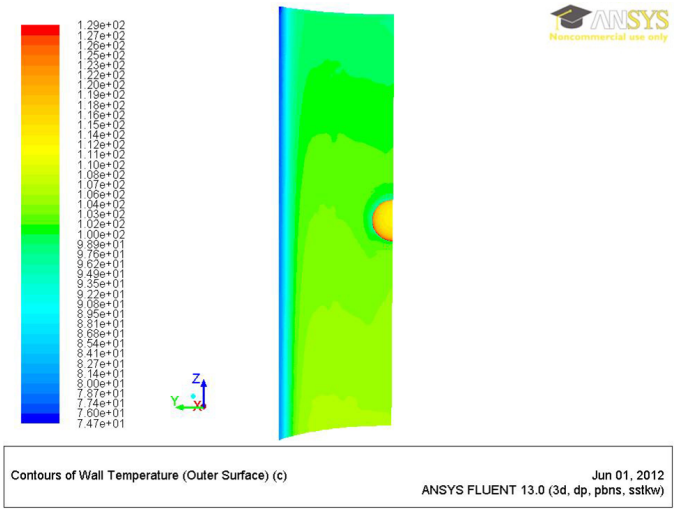

Figure 15: Temperature distribution on the inner side of the 6th tube for detachment diameter of 10 mm [2]

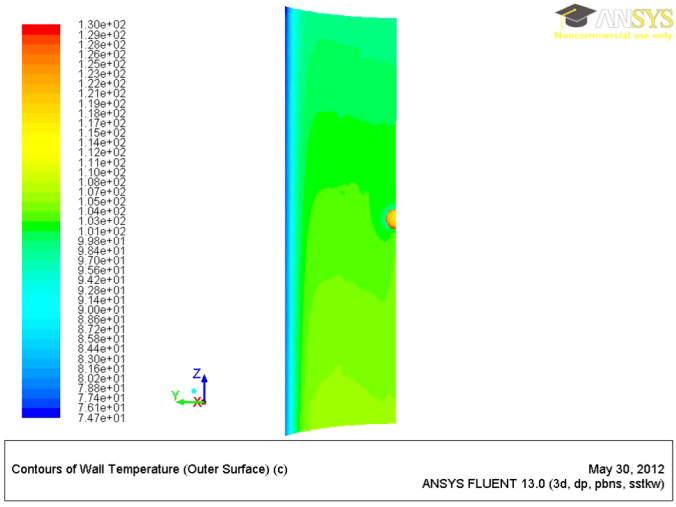

Figure 16: Temperature distribution on the inner side of the 6th tube for detachment diameter of 5 mm [2]

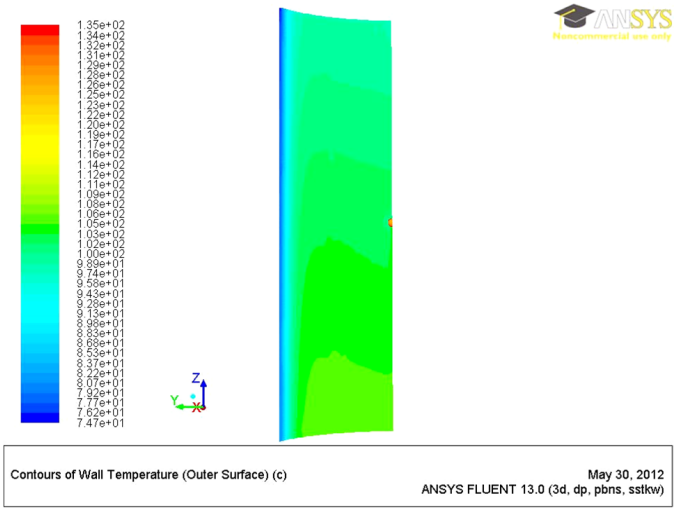

Figure 17: Temperature distribution on the inner side of the 6th tube for detachment diameter of 2 mm [2]

- It has been discovered that with smaller detachment diameter there are higher maximum values of temperature and heat flux density;
- Maximum value of heat flux density was 5.78 MW/m^2 whilst maximum value of fuel element cladding temperature was 135.2°C. Both of these values appeared in the case of the detachment diameter of 2 mm;
- The above cited maximum values are much higher than the values for the symmetrical layer;
- In none of the investigated cases was a drop of *ONBR* parameter value below 1.2 noted. This means that in none of the analyzed cases will the boiling of cooling water occur;
- The smallest value of the *ONBR* parameter occurred in the case of the detachment diameter of 2 mm, it being 1.83;
- It would be of merit to examine the heat flux density as well as the temperature for other shapes of hole detachment in subsequent calculations.

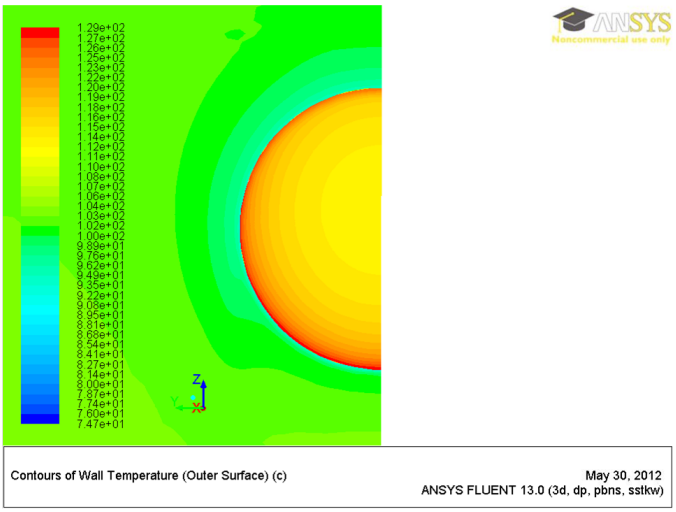

Figure 18: Temperature distribution in the hole for the detachment diameter of 10 mm

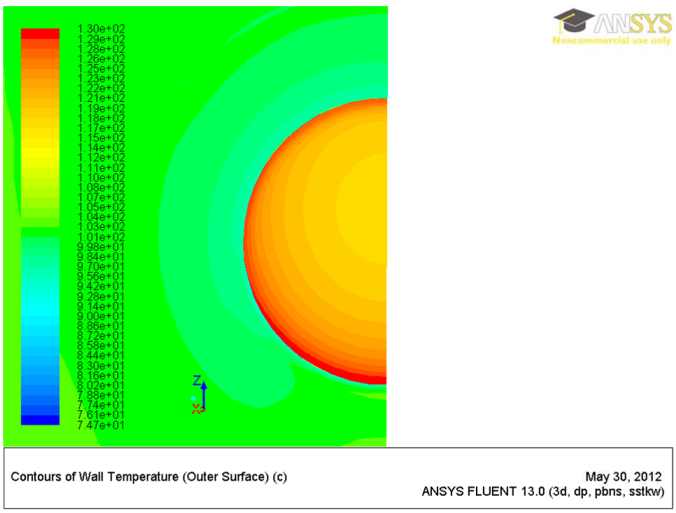

Figure 19: Temperature distribution in the hole for the detachment diameter of 5 mm

References

[1] NCBJ, Conversion of MARIA Reactor Core on MC Fuel, Annex 2011/1 to Operational Safety Report for MARIA Reactor, k. pytel Edition, in Polish (2011).

[2] S. Suchcicki, An investigation of oxide layer impact on heat transfer in maria reactor fuel elements, Master's thesis, Faculty of Power and Aeronautical Engineering, Warsaw University of Technology, in Polish (June 2012).

[3] W. Gogół, Heat Transfer. Tables and Graphs, WPW, 1991, in Polish.

[4] K. Ražnjević, Thermal Tables with Graphs, WNT, 1966, in Polish.

[5] SAS IP, Inc., ANSYS FLUENT 13.0 Documentation (2010).

[6] Operational Safety Report for MARIA Reactor, k. pytel Edition, in Polish (2009).

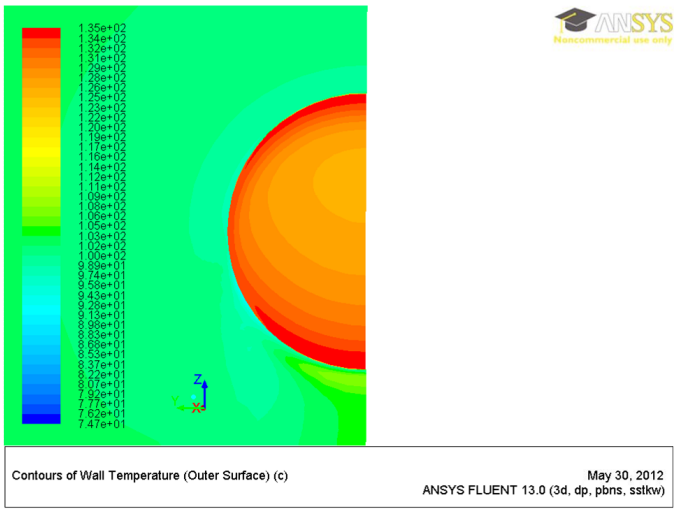

Figure 20: Temperature distribution in the hole for the detachment diameter of 2 mm

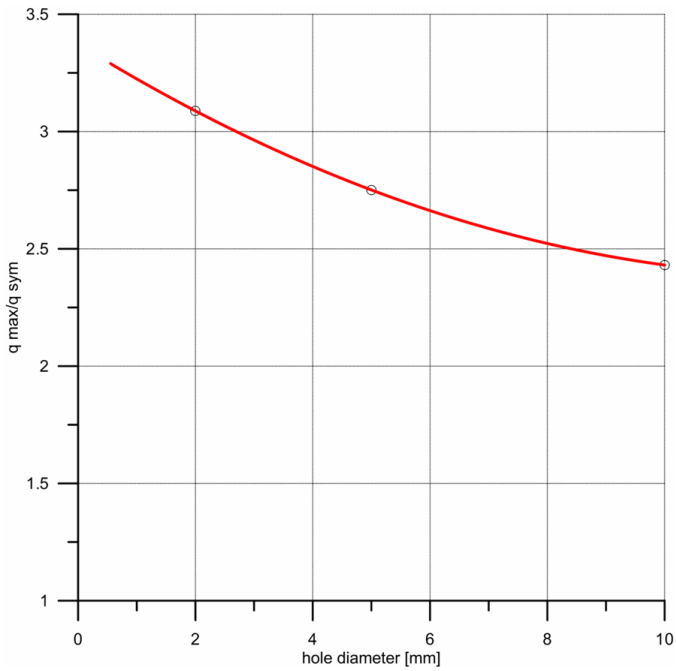

Figure 21: Relative heat flux densities as a function of hole diameter

[7] H. K. Versteeg, W. Malalasekera, An Introduction to Computational Fluid Dynamics. The finite volume method, Pearson Education Ltd., 2007.

[8] S. Wiśniewski, T. S. Wiśniewski, Heat Transfer, WNT, 2009, in Polish.

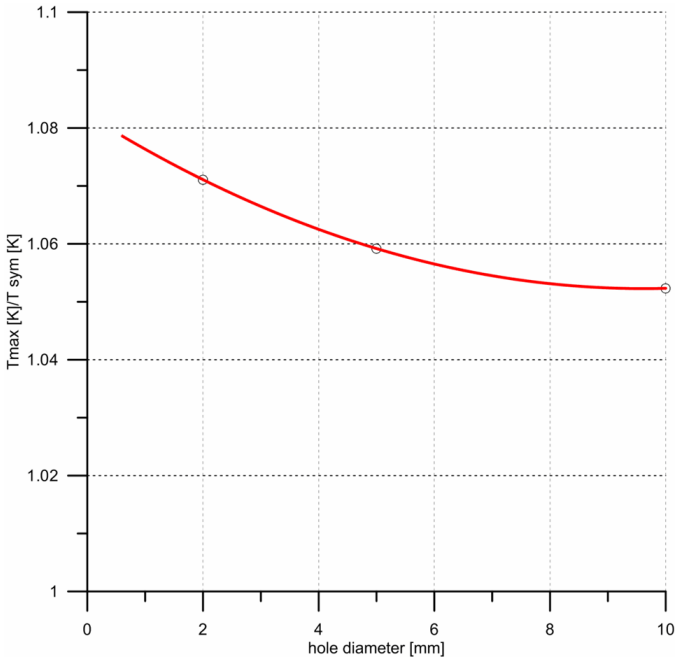

Figure 22: Relative temperatures as a function of hole diameter

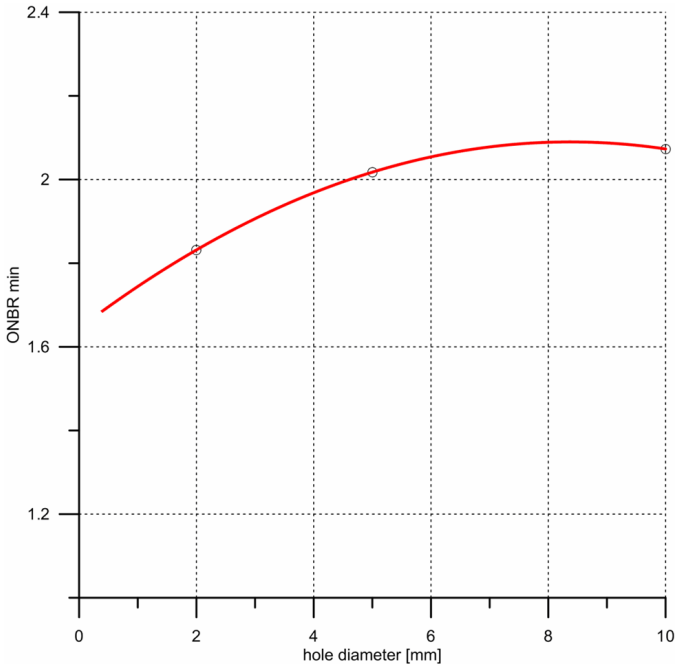

Figure 23: Minimal values of ONBR parameter for cases c), d) and e)